METEOROLOGICAL APPLICATIONS
Meteorol. Appl. **25**: 49–55 (2018)
Published online 16 August 2017 in Wiley Online Library
(wileyonlinelibrary.com) DOI: 10.1002/met.1668

Dual temperature sensors with different emissivities in radiosondes for the compensation of solar irradiation effects with varying air pressure

Sang-Wook Lee,[a] Eun Uk Park,[a,b] Byung Il Choi,[a] Jong Chul Kim,[a] Sang-Bong Woo,[a] Seongchong Park,[a] Seung Gu Yang[c] and Yong-Gyoo Kim[a]*

[a] *Division of Physical Metrology, Korea Research Institute of Standards and Science, Daejeon, Korea*
[b] *Department of Electronics, Hanbat National University, Daejeon, Korea*
[c] *Meteorological Environment Research Center, Jinyang Industrial, Ansung, Korea*

ABSTRACT: One of the challenges in temperature measurements in the upper air using a radiosonde is the correction of solar radiation effects. A prerequisite for the correction is *in situ* measurements of solar radiation. In this study, a new technique for the measurement of solar irradiation followed by the temperature correction was developed using dual temperature sensors with different emissivities. The principle is that the radiation intensity is calculated by using the temperature difference between two thermistors coated with different materials (one with graphite and the other with aluminium) and then the irradiance obtained is used for the correction. As a first stage, the effect of air pressure on the temperature correction process using dual thermistors was examined. The temperature difference between the two sensors was found to be linearly proportional only to the irradiance up to 360 W m^{-2}, regardless of air pressure from 10 to 1000 hPa at room temperature. This provides a way to calculate the irradiance by simply measuring the temperature difference between the two sensors. The calculated irradiance showed a difference of less than 45 W m^{-2} (13% of the maximum irradiance) compared to the irradiance measured with a calibrated pyranometer. The extended uncertainty of the calculated irradiance was 53.5 W m^{-2} (coverage factor $k = 2$). A reference temperature sensor in the shade was used to obtain a correction formula as a function of air pressure and calculated irradiance. When the temperature was corrected using the calculated irradiance, the extended uncertainty of the corrected temperature was 0.98 K ($k = 2$).

KEY WORDS temperature sensor; solar radiation; radiosonde; air temperature metrology; thermal metrology for climate

Received 13 December 2016; Revised 7 February 2017; Accepted 13 March 2017

1. Introduction

Accurate measurements of air temperature, humidity, pressure and wind speed/direction are of great interest to metrology as well as meteorology communities for various applications in industries, climate and weather predictions, and safety issues. Accurate measurement of the upper air mostly relies on balloon-borne radiosondes equipped with temperature and humidity sensors flying up to the lower stratosphere (about 30 km in altitude). The importance of upper air measurements has been acknowledged by the launch of the Global Climate Observing System (GCOS) Reference Upper Air Networks (GRUAN) (GCOS, 2007, 2013). Among essential climate variables, air temperature ranks as the highest priority in climate observation requirements for the GRUAN. More recently, traceable measurements on environmental parameters have been emphasized through the mutual recognition arrangement between the World Meteorological Organization (WMO) and the Bureau International des Poids et Mesures (BIPM) (WMO-BIPM, 2010). Subsequently, the Metrology for Meteorology project (Merlone *et al*., 2015) was initiated to resolve technical challenges. For traceable measurements of the temperature in the upper air, one of the challenges is the correction of the solar radiation effect. Solar radiation is well known to induce warm biases on temperature measurements in day time (Sun *et al*., 2013; Lee *et al*., 2016a). Although radiosonde manufacturers apply their own correction formula for the compensation of solar radiation effects, day time measurements of temperature deviate from each other by 1.7 K at high altitude (~32 km) according to the WMO report (Nash *et al*., 2011). Considering such deviation is less than 0.8 K at night time (Nash *et al*., 2011), some correction formulae provide inaccurate compensation for solar radiation effects. Indeed, correction values vary from 0.6 to 2.3 K at 1 kPa depending on the manufacturers (see table 7.1.2 in the WMO report) even though some of them use the same sensor type.

In situ correction of solar radiation effects on the temperature measured by radiosonde sensors requires information on the radiation intensity during flights. Previously, experimental studies have used balloon-borne pyranometers besides radiosondes to measure the solar radiation directly and then established a relationship between solar irradiance and the temperature increase by radiative heating (Philipona *et al*., 2013). However, the measurement of solar irradiance using additional pyranometers is not cost-effective and is thus limited to a specific testing region and season. Otherwise, radiation flux is calculated as a function of atmospheric conditions such as surface temperature, cloud cover, solar angle etc. (Luers, 1990, 1997). Since the solar radiation differs depending on latitude, solar elevation angle and so on, a new technique for *in situ* measurements of solar radiation is required for compensation of the solar radiation effect in a traceable manner to the International System of Units (SI).

* Correspondence: Y.-G. Kim, Division of Physical Metrology, Korea Research Institute of Standards and Science, Gajeong-ro 267, Yuseong-gu, Daejeon 34113, Republic of Korea. E-mail: dragon@kriss.re.kr

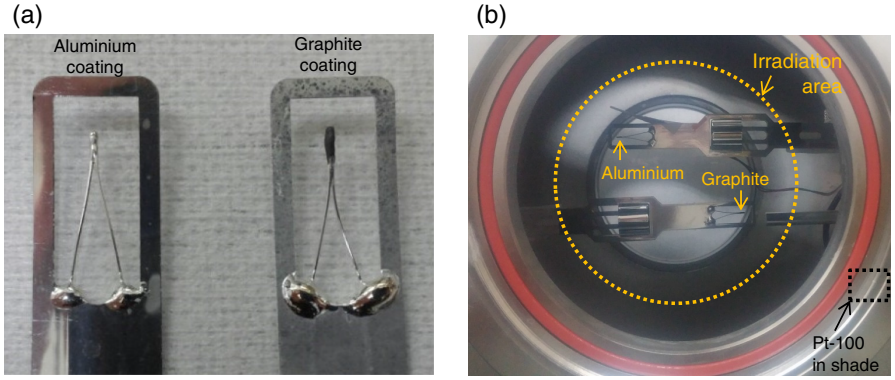

Figure 1. (a) Photograph of radiosonde temperature sensors (thermistors) coated with aluminium (left) and graphite (right). (b) Photograph of radiosonde temperature sensors coated with aluminium and graphite installed on the same incident plane inside the chamber which allows the control of air pressure and irradiation from the solar simulator. An extra Pt-100 temperature sensor is installed in the shaded area unexposed to the irradiation inside the chamber. [Colour figure can be viewed at wileyonlinelibrary.com].

This study presents the concept of dual temperature sensors having different emissivities in radiosondes for the *in situ* measurement of solar irradiance without pyranometers and then the correction of warm-biased temperature. Two thermistors are coated with either graphite or aluminium to differentiate the emissivity and then installed in a thermostatic chamber. The chamber is particularly devised to study the effect of two variables, i.e. air pressure and irradiance, among essential climate variables. Under irradiation, the temperature of the graphite-coated sensor is higher than that of the aluminium-coated sensor. The difference in the temperature between the two sensors under irradiation was investigated at varying irradiances and air pressures in order to obtain a relationship between the irradiance, the air pressure and the temperature difference. This provides a unique strategy to calculate the irradiance without pyranometers by simply measuring the temperature difference and the air pressure based on the relationship between the three parameters. The obtained irradiance and the air pressure are then used for the correction of the warm-biased temperature of each thermistor under irradiation. The experimental observations are explained using heat transfer equations.

2. Methodology

2.1. Experimental details

In order to differentiate the emissivity of thermistors used for radiosondes (RSG-20, Jinyang Industrial), either graphite or aluminium was coated on two thermistors, as shown in Figure 1(a). The emissivities of graphite and aluminium are known to be about 0.7–0.9 and 0.05–0.2, respectively (Schmidlin *et al.*, 1986; Bartl and Baranek, 2004; Machin *et al.*, 2011). Graphite- and aluminium-coated thermistors were installed on the same incident plane of irradiation inside the chamber (Figure 1(b)). A temperature sensor (Pt-100) was additionally installed in the shaded area for measuring the reference air temperature (Figure 1(b)). Details of the chamber are described in a previous report (Lee *et al.*, 2016b). In brief, the radiosonde chamber allows light transmission through quartz windows (100 mm in diameter and 10 mm in thickness) at the top and the bottom. The radiation intensity is controlled by replacing neutral density filters (FS-ND, Newport Corporation) attached to the solar simulator (LCS-100^{TM} M94011A-ES, Oriel Instruments). The nominal optical densities (d) of the neutral density filters used in this study were 0.1, 0.3, 0.5 and 1, which allow about 80, 50, 32 and 10% transmission of irradiance, respectively. In order to control and monitor the pressure in the radiosonde chamber, a solenoid valve followed by a needle valve and a pressure gauge (Model 745, Paroscientific) were used. For measurement of the irradiance, a calibrated pyranometer was first placed on the same incident plane with the two temperature sensors and then the pyranometer was removed after measurement of the irradiation to avoid any thermal disturbance in the temperature measurements under irradiation. Throughout this study, the radiosonde chamber and the radiation source were kept in a thermostatic chamber in which the temperature and relative humidity was maintained at 20 °C and 60%, respectively.

3. Results and discussion

3.1. Temperature change at various irradiances

Figure 2 shows the temperature change of graphite-coated (black curve) and aluminium-coated (grey curve) thermistors in real time upon irradiation; the irradiation starts at time $t = 0$ min. The radiation intensity is gradually increased (35.9, 122.5, 185.1, 292.7 and 356.5 W m^{-2} as in Figures 2(a), (b), (c), (d) and (e), respectively) while the air pressure is fixed at 100 kPa. As expected, the temperature variation of the two sensors from the starting point (20 °C) as well as the temperature gap between the two sensors becomes bigger as the irradiance becomes stronger. The temperature variation of the two sensors and the temperature gap between sensors at $t = 10$ min are shown in Figure 3. In our previous study, 10 min was used for the timescale of apparent equilibrium in the current chamber system (Lee *et al.*, 2016b). The temperature variation of the two sensors is apparently linearly proportional to the irradiance although that of the graphite-coated sensor is larger than that of the aluminium-coated sensor due to the difference in emissivity. Although the maximum irradiance (356.5 W m^{-2}) of the present study is not in the practical range (1500 W m^{-2}) due to the instrumental limit, it was found that the linear relationship is valid up to 1500 W m^{-2} using an independent experimental setup (Lee *et al.*, 2017). Thus, the temperature difference between the two sensors provides a clue for obtaining the irradiance without pyranometers.

The temperature variation of each sensor is governed by the heat transfer equation as follows (Schmidlin *et al.*, 1986):

$$-h\left(T_{\text{sensor}} - T_{\text{air}}\right) - \sigma\varepsilon\left(T_{\text{sensor}}^4 - T_{\text{air}}^4\right) + \varepsilon S_{\text{m}} = 0 \qquad (1)$$

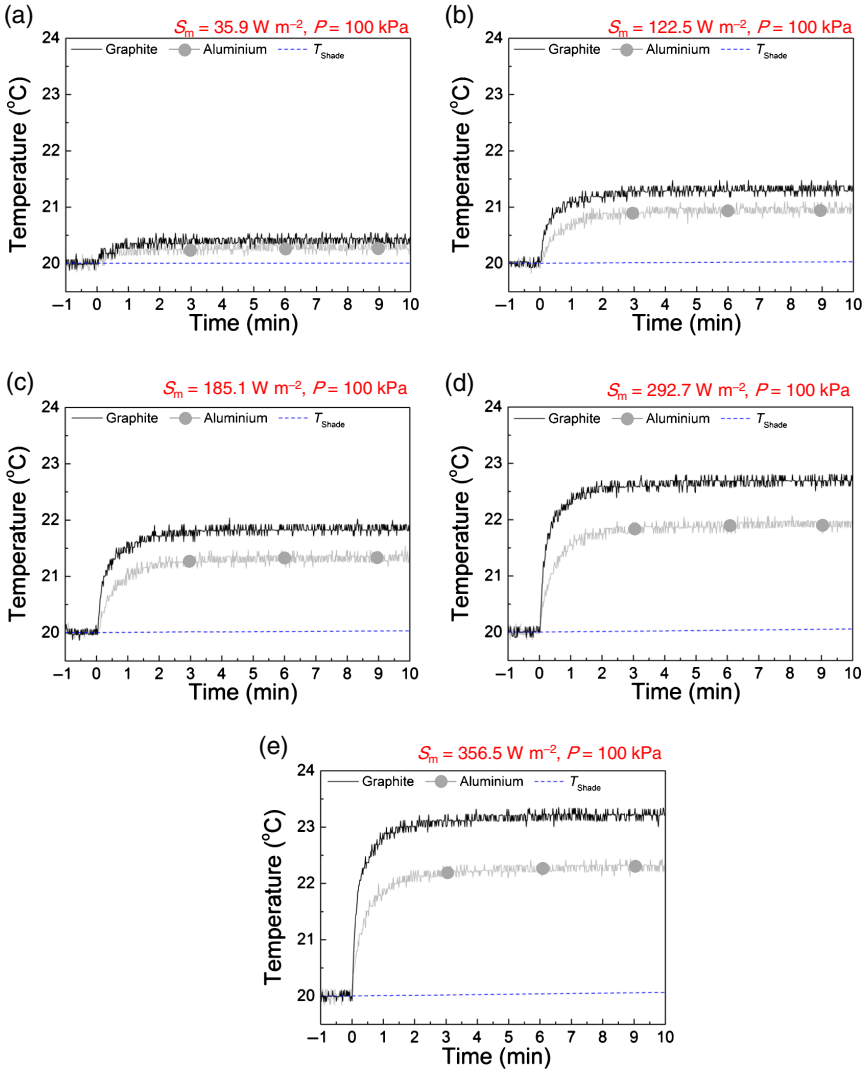

Figure 2. Temperature change of graphite-coated (black curve) thermistors and aluminium-coated (grey curve) thermistors under a fixed pressure (100 kPa) at irradiances of (a) 35.9 W m^{-2}, (b) 122.5 W m^{-2}, (c) 185.1 W m^{-2}, (d) 292.7 W m^{-2} and (e) 356.5 W m^{-2}. The dashed line is the reference temperature measured in the shade. [Colour figure can be viewed at wileyonlinelibrary.com].

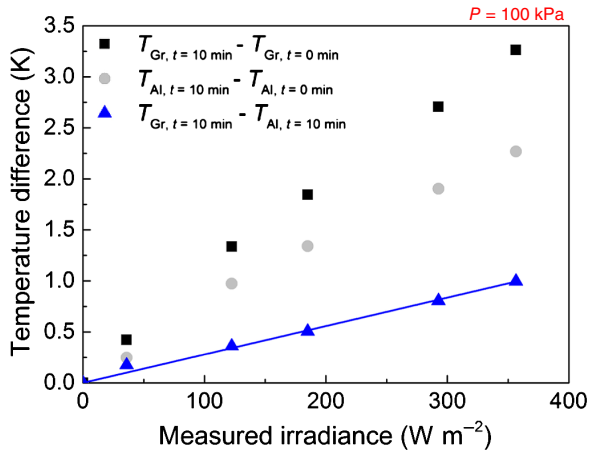

Figure 3. Temperature variation of graphite-coated (black square) and aluminium-coated (grey circle) thermistors under irradiation for 10 min at 100 kPa and the temperature difference between the two thermistors (triangle) with a linear fitting to the data (solid line). [Colour figure can be viewed at wileyonlinelibrary.com].

where h is the heat transfer co-efficient (W K^{-1}), T_{sensor} is the temperature of the sensor (K), T_{air} is the temperature measured with a reference thermometer (K), σ is the Stefan–Boltzmann constant (W m^{-2} K^{-4}), ε is the emissivity and S_m is short wave (solar) measured irradiance (W m^{-2}). Equation (1) can then be organized as:

$$\left(\frac{T_{sensor}}{T_{air}}\right)^4 + \frac{h}{\sigma\varepsilon T_{air}^3}\left(\frac{T_{sensor}}{T_{air}}\right) - \left(\frac{h}{\sigma\varepsilon T_{air}^3} + \frac{S_m}{\sigma T_{air}^4} + 1\right) = 0 \quad (2)$$

By the approximation $T_{sensor}/T_{air} \sim 1$ and thus $T_{sensor}/T_{air} = 1 + \delta$, the temperature variation of the sensor relative to the air temperature, $(T_{sensor} - T_{air})/T_{air} = \delta$, can be expressed as:

$$1 + 4\delta + \frac{h}{\sigma\varepsilon T_{air}^3}(1 + \delta) - \left(\frac{h}{\sigma\varepsilon T_{air}^3} + \frac{S_m}{\sigma T_{air}^4} + 1\right) = 0 \quad (3)$$

which gives:

$$T_{sensor} - T_{air} = \frac{1/\sigma T_{air}^3}{\left(h/\sigma\varepsilon T_{air}^3\right) + 4} S_m \quad (4)$$

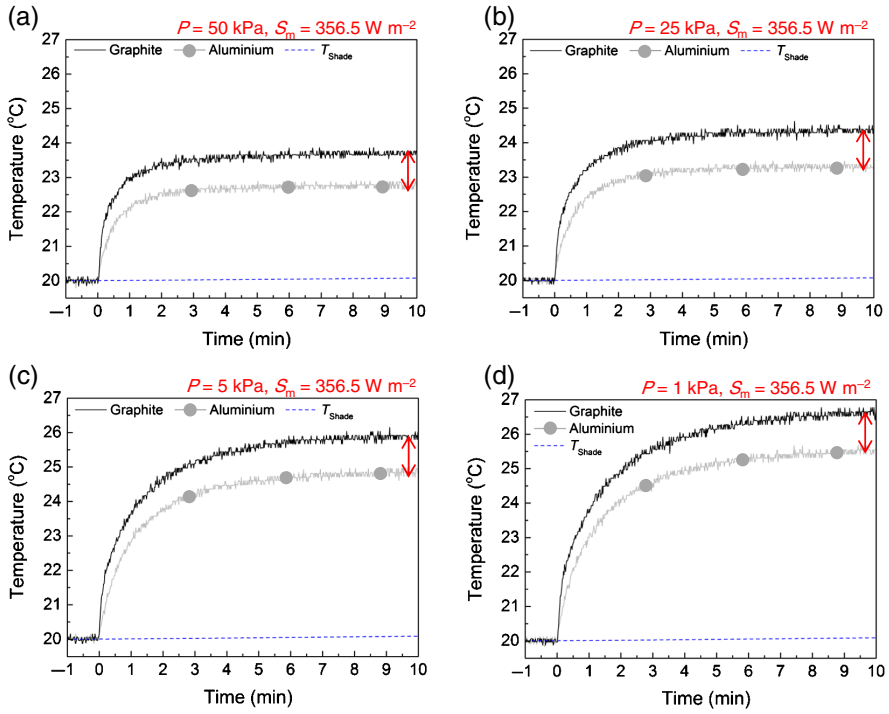

Figure 4. Temperature change of graphite-coated (black curve) and aluminium-coated (grey curve) thermistors under a fixed irradiance (356.5 W m^{-2}) at air pressures of (a) 50 kPa, (b) 25 kPa, (c) 5 kPa and (d) 1 kPa. The dashed line is the reference temperature measured in the shade. [Colour figure can be viewed at wileyonlinelibrary.com].

Therefore, the temperature variation of these sensors with respect to T_{air} should be roughly proportional to the measured irradiance (S_m) as indicated in Equation (4), and thus the temperature difference ($T_{Gr} - T_{Al}$) between the two sensors is also proportional to S_m as follows:

$$\begin{aligned}\left(T_{Gr} - T_{air}\right) - \left(T_{Al} - T_{air}\right) &= T_{Gr} - T_{Al} \\ &= \left\{ \frac{1/\sigma T_{air}^3}{\left(h/\sigma\varepsilon_{Gr}T_{air}^3\right) + 4} - \frac{1/\sigma T_{air}^3}{\left(h/\sigma\varepsilon_{Al}T_{air}^3\right) + 4} \right\} S_m \end{aligned} \quad (5)$$

in which ε_{Gr} and ε_{Al} are the emissivity of graphite-coated and aluminium-coated thermistors, respectively. This theoretical approach to the temperature difference between the two sensors is consistent with the experimental observation (triangles in Figure 3) with a linear fitting (solid line). Note that the solar irradiance is an independent factor which has nothing to do with air temperature, pressure and ventilation in the upper air. Therefore, the linear relationship will still be valid although the slope will be changed when other factors play a role. In order to obtain the irradiance by the temperature difference between two sensors, the effect of other environmental variables on the slope should be investigated. In this study, the effect of air pressure is first considered because it significantly affects the heat transfer between sensors and the surrounding air.

3.2. Temperature change at various air pressures

Since the concept of dual temperature sensors aims at the measurement of solar irradiation in the upper air using radiosondes, temperature variations of these sensors are studied in the range of upper air pressure down to 1 kPa (~30 km in altitude) as shown in Figure 4. The air pressure inside the chamber is gradually decreased (50, 25, 5 and 1 kPa in Figures 4(a), (b), (c) and (d), respectively) while the radiation intensity is fixed at 356.5 W m^{-2}. When the irradiation is started at $t = 0$, the temperature variation from the starting point (20 °C) becomes bigger as the air pressure is lowered. This can be understood because the heat transfer from the heated sensor to the surrounding air is reduced at low air pressure as previously studied (Lee *et al.*, 2016b).

In order to describe the mechanism behind this observation more qualitatively, Equation (4) is revisited, focusing on the heat transfer co-efficient (h) which is the only factor affected by the pressure (P) as follows:

$$h = kl\left(\alpha + \beta \mathrm{Re}^m\right) \quad (6)$$

where k (W m^{-1} K^{-1}) is the thermal conductivity of air, l is the length of the sensor, α and β are factors related to sensor geometry, and m is the exponent relating Reynolds number Re to h. From the relationship $\mathrm{Re} = \rho v d/\mu$ (ρ is the air density, v is the velocity of the air flow, d is a characteristic length, μ is the viscosity of air) and $\rho = P/R_{specific}T$ in which $R_{specific}$ is the specific gas constant, Equation (6) can be expressed as:

$$h = kl\left\{\alpha + \beta\left(Pvd/R_{specific}T_{air}\mu\right)^m\right\} \quad (7)$$

Therefore, when the pressure P is lowered in Equation (7), the heat transfer co-efficient h is reduced, resulting in an increase in $T_{sensor} - T_{air}$ in Equation (4); the loss of thermal energy from the sensors by convection is reduced at low air pressure and thus the temperature of the sensors is increased due to solar heating.

3.3. Calculation of irradiance by the temperature difference between dual sensors

Interestingly, even though the pressure is lowered (Figures 4(a)–(d)), the temperature gap (arrow) between two sensors seems unchanged (about 1 °C) at fixed irradiance

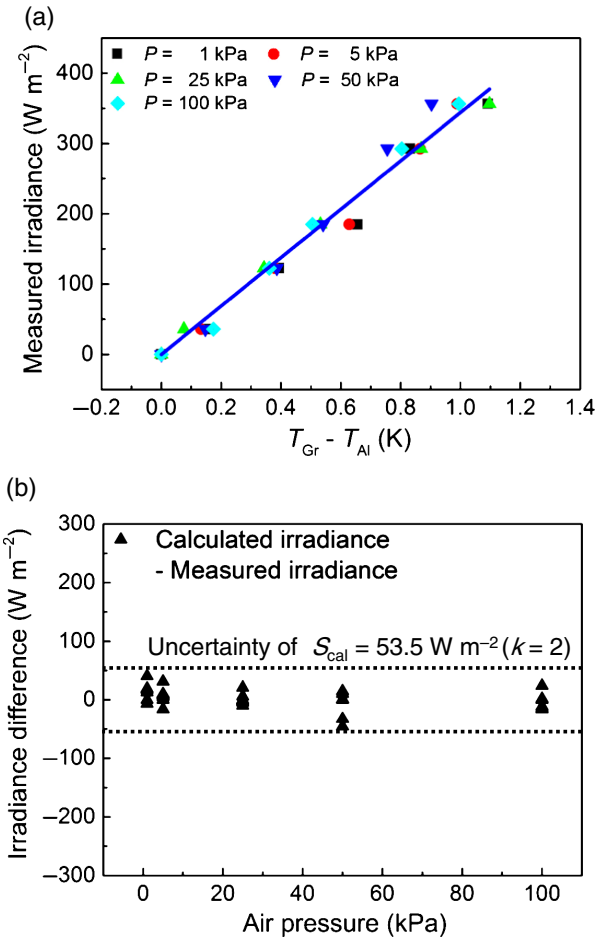

Figure 5. (a) Temperature difference between two thermistors at each air pressure corresponding to irradiance measured with a pyranometer and a linear fitting to all data (solid line). (b) The difference between the irradiance measured by the pyranometer and that calculated using Equation (8) at various air pressures. [Colour figure can be viewed at wileyonlinelibrary.com].

(356.5 W m^{-2}). A similar observation on the gap between two temperatures is also found at a lower irradiance (122.5 W m^{-2}) as shown in Figure S1. Although this observation may change depending on the ventilating condition in the upper air, the invariance of the temperature difference with respect to air pressure is valid at all tested irradiances in this chamber-based study with no ventilation (Figure S2). The temperature difference between the two sensors as a function of irradiance is shown in Figure 5(a). It is found that the temperature differences at various air pressures and irradiances can be fitted with one unifying linear function (solid line in Figure 5(a)) which is only a function of irradiance, not apparently air pressure, as follows:

$$S_{\mathrm{cal}} = a \times \left(T_{\mathrm{Gr}} - T_{\mathrm{Al}}\right) \tag{8}$$

The fitting co-efficient a (W m^{-2} K^{-1}) is 344 for this combination of thermistors. This indicates that the irradiance (S_{cal}) can be calculated when the temperature difference is obtained, irrespective of air pressure. The difference between the reference irradiance measured with a calibrated pyranometer and that calculated using Equation (8) is displayed in Figure 5(b). Under irradiation from 0 to 356.5 W m^{-2}, the difference lies within 45 W m^{-2} (13% of the maximum S in the test) irrespective of air pressure. The extended uncertainty of S_{cal} is found to be 15% ($k = 2$) which corresponds to 53.5 W m^{-2}, as is discussed in Section 3.5.

3.4. Compensation of solar irradiation

In order to obtain compensation values at a given irradiance and air pressure, the difference between the thermistor temperature (T_{sensor}) and the air temperature (T_{air}) is plotted as a function of irradiance at various air pressures. The air temperature is measured with a reference sensor (Pt-100) installed in the shaded area inside the chamber (Figure 1(b)) and thus T_{air} is replaced by T_{shade} in the following equations. In line with the theoretical considerations in Equation (4), the compensation value ($T_{\mathrm{sensor}} - T_{\mathrm{shade}}$) obtained experimentally is linearly proportional to the calculated irradiance (S_{cal}) for both graphite- and aluminium-coated thermistors, as shown in Figures 6(a) and (b), respectively. The slope of the linear fittings in Figures 6(a) and (b) is determined by the air pressure in such a way that, as the air pressure decreases, the slopes of the fittings increase. The relationship between the air pressure and the slope of the fittings for both thermistors is plotted and fitted with an exponential decay function as shown in Figure 6(c). In this way, the compensation formula for solar radiation (S_{cal}) at various air pressures (P) is expressed empirically as follows:

$$T_{\mathrm{sensor}} - T_{\mathrm{shade}} = S_{\mathrm{cal}} \times \{A + B \exp(-P/C)\} \tag{9}$$

where A, B and C are fitting co-efficients in Figure 6(c). Finally, Equation (9) can be combined with Equation (8) by replacing S_{cal} as follows:

$$T_{\mathrm{sensor}} - T_{\mathrm{shade}} = a \times \left(T_{\mathrm{Gr}} - T_{\mathrm{Al}}\right) \times \{A + B \exp(-P/C)\} \tag{10}$$

Equation (10) is the essence of this work and suggests that the irradiance can be obtained by the temperature difference between two thermistors and that the obtained irradiance can be used to give compensation values at various air pressures. Note that the A (K m^2 W^{-1}), B (K m^2 W^{-1}) and C (kPa) fitting co-efficients can be obtained by ground-based calibration facilities. In this case, the obtained A, B and C values are 0.00925, 0.00935 and 22.39271 for the graphite-coated thermistor and 0.00654, 0.00902 and 21.92579 for the aluminium-coated thermistor, respectively. For both graphite- and aluminium-coated sensors, the difference between the measured air temperature in the shade and the corrected temperature by Equation (10) is plotted as a function of the calculated irradiance in Figure 7. The mean and standard deviation of the difference between the reference temperature and the corrected temperature are −0.03 and 0.25 K, respectively. The difference is mostly due to deviations of the data from the fitting in Figure 5(a). Nevertheless, it is important to note that the concept of dual sensors with different emissivities for measuring the irradiance and thereby compensating the effect of irradiation is demonstrated using ground-based facilities. This technique provides the traceability to SI in the compensation of the solar irradiation and also enables *in situ* compensation, irrespective of region, solar angle, atmospheric condition etc. Therefore, the study on this technique will be extended further in the future to incorporate the effect of ventilation and low temperature mimicking the upper air environment.

3.5. Uncertainty

The uncertainties of the pressure, the irradiance and temperature are listed in Table 1. The uncertainty factors of the pressure considered inside the chamber are the calibration of the pressure gauge, the repeatability and the reproducibility, which are 0.015, 0.2 and 0.2%, respectively (coverage factor $k = 1$). The combined uncertainty $u_{\mathrm{c}}(P)$ of the pressure is 0.3% ($k = 1$) in

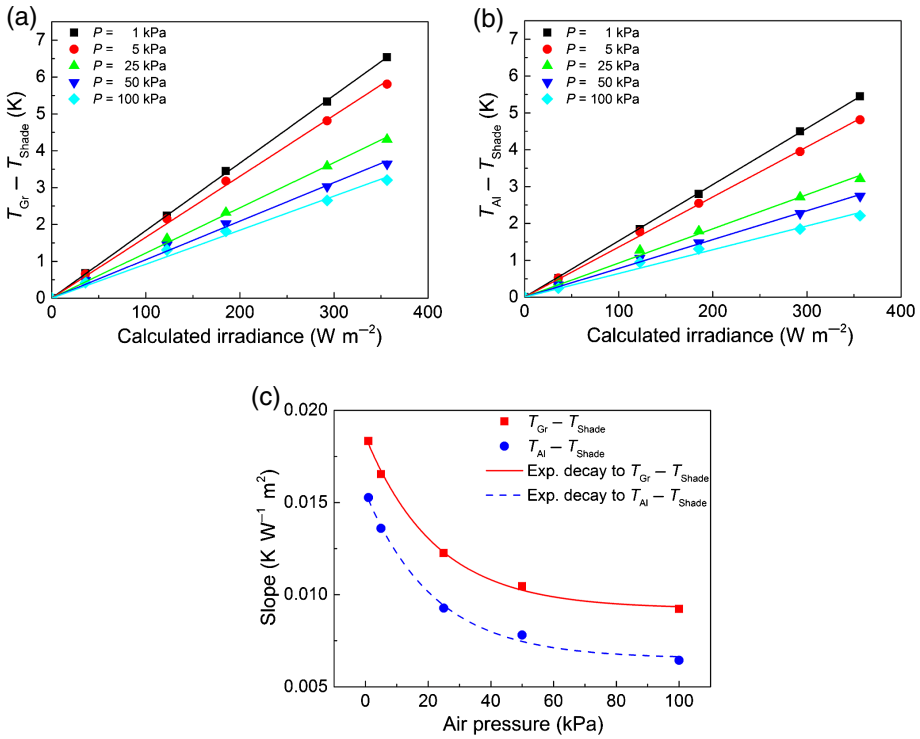

Figure 6. (a) The temperature difference between the graphite-coated sensor and the Pt-100 sensor in the shade as a function of irradiance and linear fittings (lines) at various air pressures. (b) The temperature difference between the aluminium-coated sensor and the Pt-100 sensor in the shade as a function of irradiance and linear fittings (lines) at various air pressures. (c) The slope of fittings in (a) and (b) as a function of air pressure and exponential fittings to the data. [Colour figure can be viewed at wileyonlinelibrary.com].

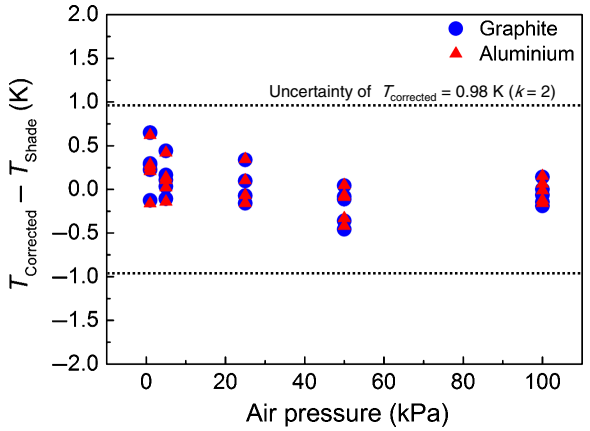

Figure 7. The difference between temperature in the shade and corrected temperature based on the calculated irradiance in Figure 5(b). [Colour figure can be viewed at wileyonlinelibrary.com].

the 1–100 kPa range. For the measured irradiance (S_m) in the chamber, the calibration of the pyranometer and the spatial gradient in the chamber are considered and the relative uncertainty of each factor is 0.2 and 0.6% at 356.5 W m^{-2}, respectively. Therefore, the combined relative uncertainty $u_{c,r}(S_m)$ of the measured irradiance is 0.63% ($k = 1$). The uncertainty of the calculated irradiance $u_{c,r}(S_{cal})$ by the dual thermistors includes the uncertainty of the temperature difference between the dual thermistors as follows:

$$u_c^2\left(S_{cal}\right) = \left\{\frac{\partial S_{cal}}{\partial\left(T_{Gr} - T_{Al}\right)}\right\}^2 u^2\left(T_{Gr} - T_{Al}\right) \qquad (11)$$

The right side is calculated using Equation (8) and results in 7.5% ($k = 1$). Note that the uncertainty of the measured irradiance ($u_c(S_m)$) is incorporated into $u_c(S_{cal})$ *via* $u(T_{Gr} - T_{Al})$ as shown in Table 1. Therefore, the combined relative uncertainty in the calculated irradiance by the dual thermistors ($u_{c,r}(S_{cal})$) is 7.5% ($k = 1$) at $S_{cal} = 356.5$ W m^{-2} at room temperature.

The uncertainty of the corrected temperature $\left(u^2_{c,\,cor}\left(T_{sensor}\right)\right)$ is expressed using Equation (10) as follows:

$$u^2_{c,\,cor}\left(T_{sensor}\right) = \left(\frac{\partial T_{sensor}}{\partial T_{shade}}\right)^2 u_c^2\left(T_{shade}\right) + \left(\frac{\partial T_{sensor}}{\partial P}\right)^2 u_c^2(P) + \left(\frac{\partial T_{sensor}}{\partial S_{cal}}\right)^2 u_c^2\left(S_{cal}\right) \qquad (12)$$

The first, second and third terms on the right are responsible for the uncertainty of the reference temperature, the compensation of pressure and the compensation of irradiation effects, respectively, and are calculated to be 45, 4 and 486 mK at $k = 1$, respectively. Therefore, the combined uncertainty of the corrected temperature is 490 mK ($k = 1$) at $S_{cal} = 356.5$ W m^{-2} and $P = 1$–100 kPa at room temperature.

4. Conclusions

A new technique using dual temperature sensors with different emissivities for the measurement and compensation of solar irradiance was explored. Two thermistors used for radiosondes were coated with either graphite or aluminium to differentiate the emissivity. The temperature variation of the graphite-coated sensor under irradiation was larger than that of the aluminium-coated sensor due to the high emissivity of graphite. In general, the temperature variation of these sensors

Table 1. Uncertainty of pressure, irradiance and temperature.

Uncertainty of pressure	Standard uncertainty (%)
Calibration	0.015
Repeatability	0.2
Reproducibility	0.2
Combined uncertainty, $u_c(P)$	0.3
Uncertainty of irradiance	(%)
Uncertainty of the measured irradiance, $u_{c,r}(S_m)$	0.63
Calibration of pyranometer	0.2
Spatial gradient in test section	0.6
Uncertainty of calculated irradiance, $u_{c,r}(S_{cal})$	7.5
Uncertainty of $T_{Gr} - T_{Al}$, $\frac{\partial S_{cal}}{\partial (T_{Gr} - T_{Al})} \times u_c \left(T_{Gr} - T_{Al}\right)$	7.5
Uncertainty of temperature	(mK)
Uncertainty of T_{Gr}, $u(T_{Gr})$	57
Repeatability of thermistor	40
Uncertainty due to measured irradiance, $\frac{\partial T_{Gr}}{\partial S_m} \times u_c \left(S_m\right)$	40
Uncertainty of T_{Al}, $u(T_{Al})$	53
Repeatability of thermistor	40
Uncertainty due to measured irradiance, $\frac{\partial T_{Al}}{\partial S_m} \times u_c \left(S_m\right)$	34
Uncertainty of $T_{Gr} - T_{Al}$, $u(T_{Gr} - T_{Al})^2 = u(T_{Gr})^2 + u(T_{Al})^2$	78
Uncertainty in temperature correction, $u_{c,cor}(T_{sensor})$	490
Uncertainty of T_{shade}, $u_c(T_{shade})$	45
Calibration of Pt-100	25
Reading of Pt-100	10
Repeatability of Pt-100	5
Spatial gradient	35
Compensation of pressure, $\frac{\partial T_{sensor}}{\partial P} \times u_c (P)$	4
Compensation of irradiance, $\frac{\partial T_{sensor}}{\partial S_{cal}} \times u_c \left(S_{cal}\right)$	486

becomes larger when the air pressure is lowered because the convectional heat transfer from the sensors to the surrounding air is reduced. The temperature difference between the two sensors was found to be approximately linearly proportional to the irradiance, irrespective of air pressure. Using this relationship, the irradiance was calculated by simply measuring the temperature difference between the two sensors at various air pressures. The compensation value was then obtained empirically based on the calculated irradiance as expressed in Equation (10). The mean and standard deviation of the difference between the reference temperature and the corrected temperature of the two sensors were −0.03 K and 0.25 K, respectively. The extended uncertainty of the corrected temperature ($u_{c,\,cor}(T_{sensor})$) was 0.98 K. The main contributing factor to $u_{c,\,cor}(T_{sensor})$ was the repeatability of the thermistors; no smoothing process was applied for removing noise. The dual-thermistor-based technique provides a simple yet efficient way to compensate the solar radiation effect on the temperature sensors of radiosondes. In future studies, more environmental parameters such as ventilation and low temperature will be considered for the practical application of the dual sensor technique which may enable *in situ* compensation of solar radiation in the upper air.

Acknowledgements

This work was supported by the Korea Research Institute of Standards and Science under the project Hidden Champion Fostering Program grant 16011205. This work was partly supported by the Ministry of Trade, Industry and Energy (MOTIE, Korea) under Industrial Technology Innovation Program no. 10067387, High Speed and High Precision Radiosonde.

Supporting information

The following material is available as part of the online article:

Figure S1. Temperature change of aluminium-coated (grey curve) and graphite-coated (black curve) thermistors under a fixed irradiance (122.5 W m^{-2}) at air pressures of (a) 100 kPa, (b) 50 kPa, (c) 25 kPa, (d) 5 kPa and (e) 1 kPa. The dashed line is the reference temperature measured in the shade.

Figure S2. The invariance of the temperature difference with air pressure at the tested irradiance.

References

Bartl J, Baranek M. 2004. Emissivity of aluminium and its importance for radiometric measurement. *Meas. Phys. Quant.* **4**: 31–36.

GCOS. 2007. GCOS Reference Upper-Air Network (GRUAN): justification, requirements, siting and instrumentation options. WMO/TD 1379. World Meteorological Organization: Geneva. https://www.wmo.int/pages/prog/gcos/Publications/gcos-112.pdf (accessed 13 July 2017).

GCOS. 2013. The GCOS Reference Upper-Air Network (GRUAN) Guide. GCOS-171. World Meteorological Organization: Geneva. https://www.wmo.int/pages/prog/gcos/Publications/gcos-171.pdf (accessed 13 July 2017).

Lee S-W, Kim JC, Choi BI, Woo S-B, So JW, Yang SG, *et al.* 2016a. Development of a double cap on the humidity sensor in radiosondes for improving ventilation. *Meteorol. Appl.* **23**: 35–39.

Lee S-W, Choi BI, Kim JC, Woo S-B, Park S, Yang SG, *et al.* 2016b. Importance of air pressure in the compensation for the solar radiation effect on temperature sensors of radiosondes. *Meteorol. Appl.* **23**: 691–697.

Lee S-W, Park EU, Choi BI, Kim JC, Woo S-B, Park S, *et al*. 2017. Correction of solar irradiation effects on the air temperature measurement using a dual-thermistor radiosonde at low-temperature and low-pressure. *Meteorol. Appl*. In Press.

Luers JK. 1990. Estimating the temperature error of the radiosonde rod thermistor under different environments. *J. Atmos. Oceanic Technol.* **7**: 882–895.

Luers JK. 1997. Temperature error of the Vaisala RS90 radiosonde. *J. Atmos. Oceanic Technol.* **14**: 1520–1532.

Machin G, Castro P, Levick A, Villamañán MÁ. 2011. Temperature effects of imperfectly formed metal-ingots in high temperature fixed point crucibles. *Measurement* **44**: 738–742.

Merlone A, Lopardo G, Sanna F, Bell S, Benyon R, Bergerud R, *et al.* 2015. The MeteoMet project – metrology for meteorology: challenges and results. *Meteorol. Appl.* **22**: 820–829.

Nash J, Oakley T, Vömel H, Li W. 2011. WMO Intercomparisons of high quality radiosonde systems. WMO/TD 1580, Yangjiang, China, 12 July – 3 August 2010. World Meteorological Organization: Geneva. https://www.wmo.int/pages/prog/www/IMOP/publications/IOM-107_Yangjiang.pdf (accessed 13 July 2017).

Philipona R, Kräuchi A, Romanens G, Levrat G, Ruppert P, Brocard E, *et al.* 2013. Solar and thermal radiation errors on upper-air radiosonde temperature measurements. *J. Atmos. Oceanic Technol.* **30**: 2382–2393.

Schmidlin FJ, Luers J, Huffman P. 1986. Preliminary estimates of radiosonde thermistor errors. NASA Technical Paper 2637. National Aeronautics and Space Administration: Washington, DC; 15. http://ntrs.nasa.gov/archive/nasa/casi.ntrs.nasa.gov/19870002653.pdf (accessed 13 July 2017).

Sun B, Reale A, Schroeder S, Seidel DJ, Ballish B. 2013. Toward improved corrections for radiation-induced biases in radiosonde temperature observations. *J. Geophys. Res. Atmos.* **118**: 4231–4243.

WMO-BIPM. 2010. Measurement challenges for global observation systems for climate change monitoring. WMO/TD-No. 1557. World Meteorological Organization: Geneva. https://library.wmo.int/pmb_ged/wmo-td_1557.pdf (accessed 13 July 2017).

